NRIAG JOURNAL OF ASTRONOMY AND GEOPHYSICS
2025, VOL. 14, NO. 1, 36–50
https://doi.org/10.1080/20909977.2025.2449790

Geological and geophysical evaluation of the subsurface conditions for establishing new dwelling area East New Cairo City

N. Tawir[a,b], A. Lethy[c], M. Abbas[c], TH Abdel Fattah[b], M. Al- Maghraby[b] and M. Osman[b]

[a]Geology Department, Faculty of Science, University of Kordofan, El-Obied, Sudan; [b]Geology Department, Faculty of Science, Alexandria University, Alexandria, Egypt; [c]National Research Institute of Astronomy and Geophysics, EL Marsad Street 1, Helwan, Cairo

ABSTRACT

An integrated geological and geophysical study utilising electrical resistivity tomography (ERT) and seismic refraction tomography (SRT) was carried out in a new residential area located northeast of New Cairo City and south of the Suez-Cairo Road. The purpose was to characterise the subsurface layer distribution, lithology, and geometry of faults . Initial surface geological mapping identified traces of some faults. Stratigraphically, the study area comprises sedimentary rocks and local basaltic flow outcrops ranging in age from the Middle Eocene (Mokattam Formation) to the Upper Miocene (Hagul Formation). ERT and SRT data were acquired along 15 closely spaced profiles oriented to intersect the expected surface fault zones. ERT delineated electrical conductive zones situated at different depths and composed of shale and altered basalt. Meanwhile, three layers were detected based on velocity values obtained from SRT data analysis. The ERT and SRT results successfully elucidated the fault configuration and its locations, providing crucial information for construction planning. Major structures were concealed and only outlined by the integrated ERT/SRT surveys. This study shows heterogeneous soil conditions and fault damage zones, which may impact some parts of the study area. The study's findings , offering vital information for safe and effective construction planning.

ARTICLE HISTORY
Received 18 September 2024
Revised 20 November 2024
Accepted 31 December 2024

KEYWORDS
SRT data; ERT data; integrated geophysical methods; East New Cairo; Egypt

1. Introduction

Egypt has experienced a revolutionary development in various sectors, including the construction of new cities. Geotechnical studies are critical for new urban development, ensuring that construction is safe, sustainable, and resilient to environmental factors. These studies examine soil stability, groundwater conditions, and seismic risks, providing essential data to guide engineering and architectural decisions. Geotechnical studies are usually performed on soil sample in the lab or in the field using invasive methods such as cone penetration tests and standard penetration tests or using non-invasive geophysical methods.

The most significant benefit of geophysical technologies is their non-destructive and non-invasive nature, ensuring no harm to subterranean structures and materials (Reynolds 2011; Plati et al. 2020). This aspect of geophysical surveys has made them increasingly popular for identifying structural geology, especially in engineering and environmental studies. The efficiency gains in collecting and interpreting near-surface geophysics data have made geophysical methods almost appropriate for various project applications (Steeples 2001). In addition, the geophysical approach is preferred because it is inexpensive, has a quick turnaround time, and is compatible with various subsurface materials (Lech et al. 2020).

The electrical resistivity approach can determine the thickness of bedrock in sedimentary layers and identify the contacts between sediment and bedrock (Sibul et al. 2017).

The seismic surveyor uses the field data analysis to produce a profile that displays the depth of the underground composition and a good idea of what materials they consist of (Ayolabi et al. 2009; Igboekwe and Ohaegbuchu 2011; Okiongbo et al. 2011). One of the purposes of examining seismic wave velocities is to investigate and analyse the soil's elastic properties and its vertical and horizontal distribution.

The study area belongs to the New Cairo district, established in 2000, with a total area of about 250 km^2 and a targeted population of four million residents (Hassan et al. 2022). The city has a variety of land uses, including residential, commercial, industrial, and service areas. The study area, with its many geological structures, directly affects the construction settlement and stability.

This study aims to identify the suitability of the study area for construction and future environmental constraints. The procedure for obtaining subsurface information in this study depends on a geologic field survey, followed by the application of modern geophysical techniques (Electrical Resistivity Tomography and Seismic Refraction Tomography) to identify

CONTACT N. Tawir elnazeerh@gmail.com Geology Department, Faculty of Science, University of Kordofan, PO Box 160- El-Obeid 51111, Sudan

subsurface lithologic units, characterise the subsurface layers distribution, and prove or disprove the existence and extensions of faults.

Minor parts of the faults were exposed and observed during the geological fieldwork, while the major parts were inferred but not observed.

2. Geological settings

The study area is located northeast of New Cairo City and south of the Suez-Cairo Road (Figure 1). It lies between latitudes 30° 4' 12" and 30° 4' 55" N and longitudes 31° 27' 18" E and 31° 28' 30" E. The Ring Road borders it on the west, the Gebel ElAnqaabiya Road on the east, the Cairo-Suez desert route on the north, and the El-Qattamiya-Ain El-Sokhna Road on the south. The area between the Suez-Cairo district and the El-Sukhna-Qattamiya district contains sedimentary rocks and some patches of basaltic sheets. According to studies by Said (1962) and Abdel-Aal (1982) these rocks range in age from the Middle Eocene (Mokattam Formation) to the Upper Miocene (Hommath Formation).

The Eocene succession overlays unconformably on the Upper Cretaceous beds.

Oligocene rocks are the most prominent units in the region east of Cairo City, between the Cairo-Suez and Qattamiya-El Sukhna districts (Figure 2). The Oligocene sequence is divided into top loose sands

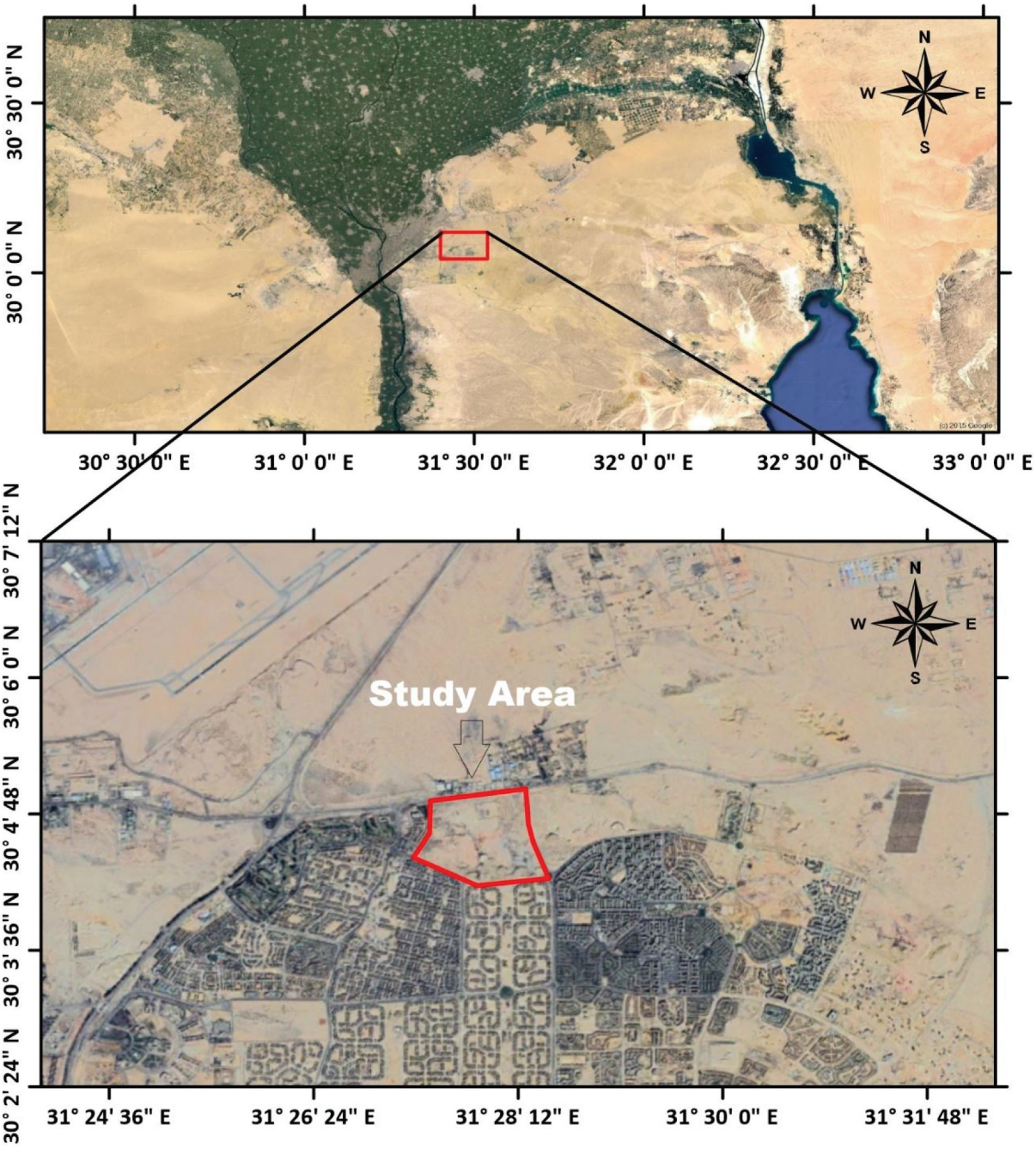

Figure 1. Location of the study area.

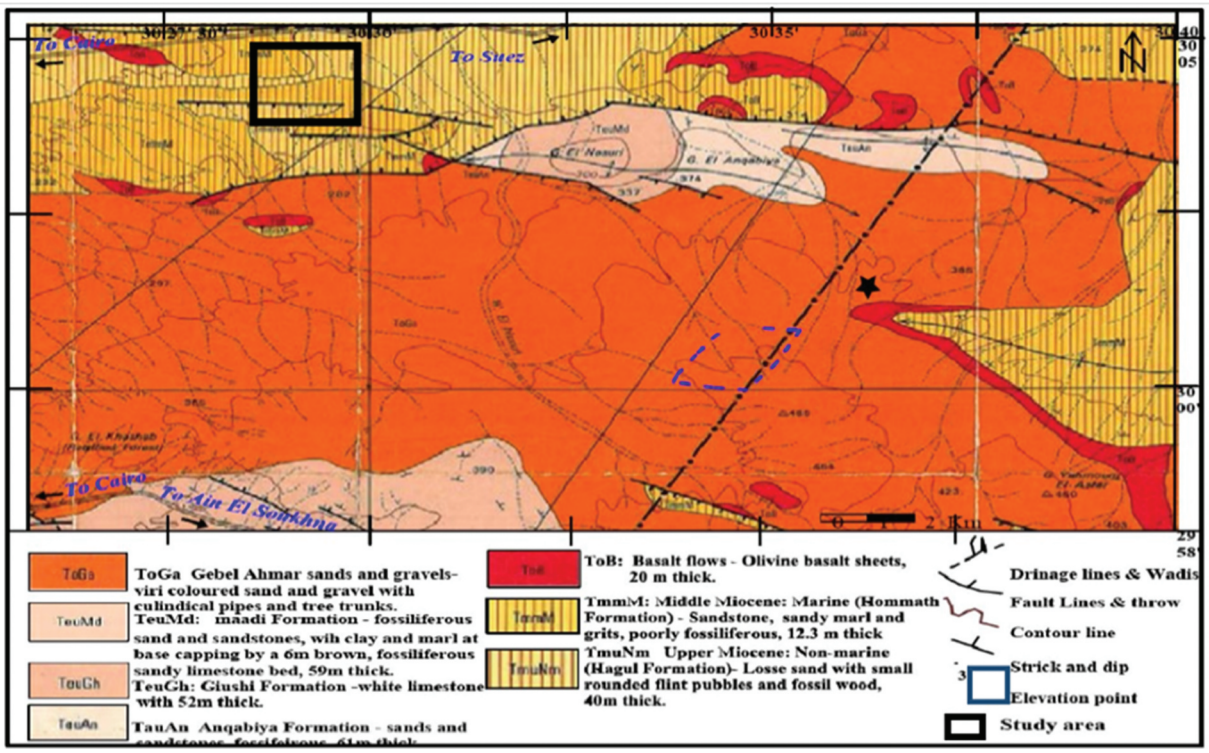

Figure 2. Geological map of the New Cairo and its environs shows the distribution of the rock units and geological structures. Black box defines borders of the study area.

and gravels, represented by the Gebel Ahmer Formation and base basaltic sheets at the top (Said 1962; Moustafa and Abd-Allah 1991; Sakr et al. 2022).

Oligocene rocks are often covered with unconformable Miocene deposits. The Miocene sequence comprises two units: the marine Miocene sediments at the base (Hommath formation) and the non-marine Miocene sediments at the top (Hagul Formation) (Figure 2). An unconformity surface separates these two units from one another (Ismail and Abdelghany 1999).

The Oligocene sediments are controlled by the dominated structures (Moustafa and Abdel Tawab 1985). These sediments are typically found in structural lows and are surrounded by NW-oriented faults (Moustafa 2010) and intersected by faults striking NW-SE, indicating the reactivation of these faults following the deposition of the rocks (Gamal et al. 2021).

Throughout these periods, NW-SE and NE-SW faults shaped the area, with reactivation during the Oligocene and Miocene due to the tectonic activity of the Red Sea rifting.

2.1. Field geological mapping

Field geological mapping involves a systematic approach to understanding the geology of an area, incorporating both surface and subsurface data. First, the published geological and borehole data is projected and organised into a GIS database, to interpret the subsurface geology through both horizontal and vertical plans. Several site visits were performed, during which surface features were observed and the outcrop locations were recorded. Each rock unit is carefully described, with thickness measurements with detailed notes on the primary and secondary structures. The field data is then converted into the GIS database, creating new layers to support various geological maps. Finally, integrating this surface data with structural cross-sections provides a 3D model of the area's fault architecture. Several faults were indicated at different locations around the study area (Figure 3). Only small parts of the faults were revealed during the geological survey, therefore there was a need to apply geophysical techniques to verify the faults and to detect the hidden parts.

Most faults mapped in the area were created or reactivated during the Red Sea rifting in the Oligo-Miocene period. This is supported by the thickening of the Miocene sediments on the side of these faults, which moved downward. Furthermore, the Miocene sediments exhibited noticeable deformation characterised by convolute bedding. Some of these faults have been reactivated from the Miocene period to the present, leading to moderate-to-low seismic events. However, faults that have experienced movement one or more times in the past 120,000 years are identified as active faults and are likely to move again (Ismail and Abdelghany 1999). The most common indication of active faults is their repeated breaking of the earth's surface, emphasising the urgency of our research.

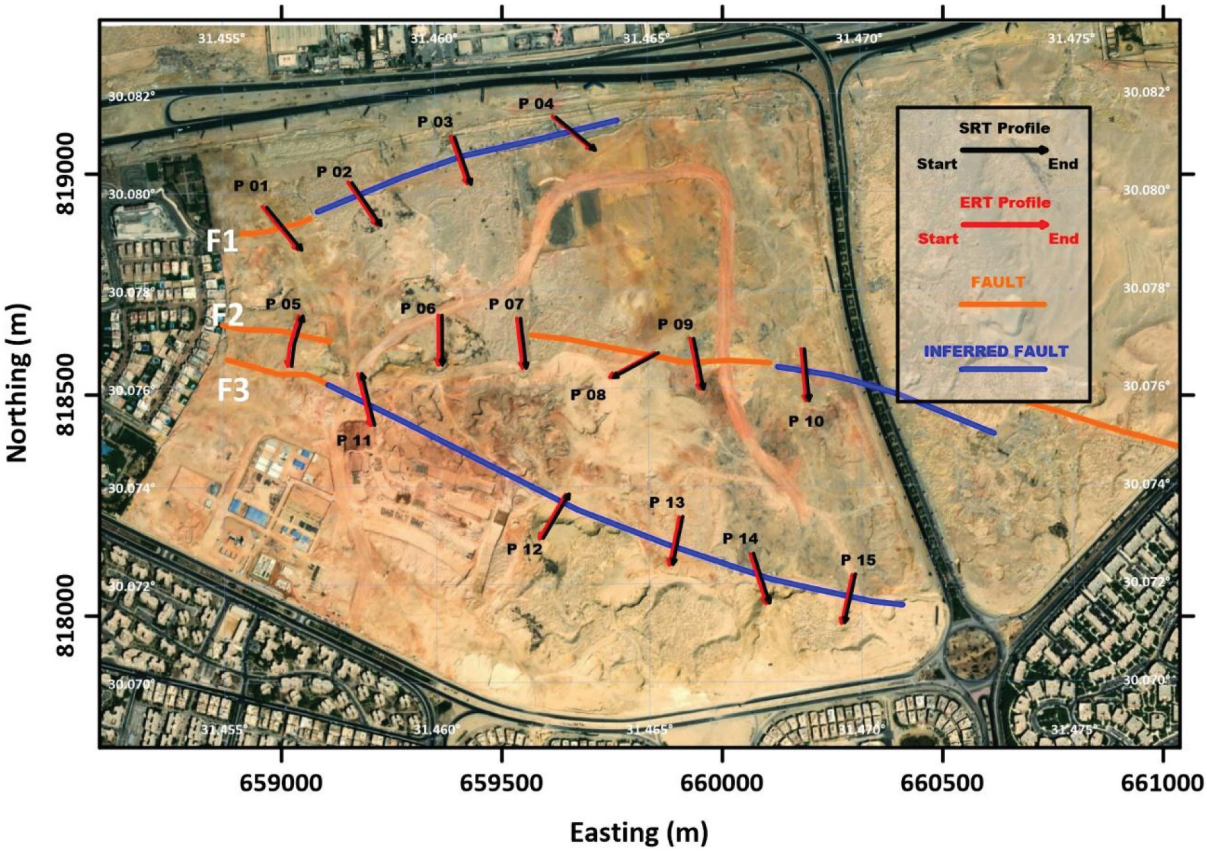

Figure 3. Location of the identified faults and orientation of geophysical profiles in the investigated site. Minor parts of the faults (orange solid lines) were exposed and observed during the geological field work, while the major parts (blue solid lines) were inferred but not observed. The black lines represent the SRT profiles while the red lines represent the ERT profiles.

2.2. Geomorphology

The study area exhibits varying topography, with a higher elevation of 420 m above mean sea level (AMSL) in the southeastern boundary and a lower elevation of 142 m AMSL towards the northwestern boundary (Hassan et al. 2022). A prominent topographic feature in the area is Geble Ahmar, which exerts significant influence over a large expanse of New Cairo City.

3. Methodology

3.1. Electrical resistivity tomography

3.1.1. Method statement

Electrical Resistivity tomography (ERT) is a crucial advancement in the traditional sounding method. The method is rooted in Ohm's Law (V = IR), where resistivity (R) represents the intrinsic ability of geological materials to resist current flow. ERT captures variations in resistivity that can indicate different rock types, water content, pore space, and temperature conditions. It offers enhanced data quality and resolution and provides continuous 2D-dimensional resistivity models. This study specifically utilised this technique due to its high-resolution capability in identifying near-surface features for engineering and environmental applications (Elkafrawy et al. 2021).

In practice, an ERT survey involves setting up a series of electrodes along the area of interest. By sending an electrical current through electrodes placed on the ground surface and measure the voltage response at different points, the resistivity distribution at various depths can be estimated. Various electrode arrays can be used in ERT survey, each with specific advantages and disadvantages. The Wenner Array has evenly spaced electrodes and is known for its simplicity and good sensitivity to vertical changes. However, it provides limited horizontal resolution, making it less ideal for detecting lateral resistivity changes. The Schlumberger Array with variable electrode spacing, is suitable for deep investigations. It has a high sensitivity to vertical changes but requires more field setup.

The Dipole–Dipole Array is sensitive to lateral resistivity changes, making it suitable for mapping shallow, horizontal variations. However, it can be more affected by noise and generally has less vertical resolution. Meanwhile, Pole–Dipole Array has a high lateral resolution. This array is effective in resolving complex near-surface variations but requires a remote electrode for consistent measurements, adding logistical challenges and is more sensitive to noise.

3.1.2. ERT data acquisition

Syscal-Pro were used to conduct the measurements for the current study. Fifteen 2D profiles were performed with a total length of 115 m (equivalent to a depth of investigation of nearly 25 m) and electrode separation of 5 m. The spatial distribution of the ERT profiles is shown in (Figure 3). The purpose was to locate the subsurface faults' extension and the subsurface layers' distribution and types. Topographic values of measuring points were accurately determined along the ERT profiles, and the ground elevation was incorporated into the ERT data inversion process.

3.1.3. ERT data processing

The field survey data must be of comparable quality to create a better model and processed before being used in the interpretation.

The measured resistivity values were carefully analysed using RES2DINV software, specifically designed to create two-dimensional resistivity models of the subsurface. To ensure data quality and point distribution, the measured data was graphed as "Apparent Resistivity Pseudo-sections". Using the "Least-Squares Approach", the processed apparent resistivity data were converted into true modelled 2D resistivity sections. The colour palette of the sections varies according to the calculated resistivity values. The high resistivity values are indicated by the red colours and their gradient (resistive layer or body). In contrast, the blue colour and its gradient indicate low resistivity values (conductive layer or body). This thorough data processing guarantees the accuracy of our results.

The Electrical Resistivity Tomography (ERT) data were inverted line by line. To facilitate the correlation among different ERT sections, a unified colour scale (pallet) was applied to all ERT sections. This colour scale helps define specific resistivity ranges for each lithologic type.

3.2. Seismic refraction tomography (SRT)

3.2.1. Method statement

Active seismic methods include seismic reflection, refraction, tomography, vertical seismic profiling (VSP), crosshole and downhole seismic, surface wave methods (e.g. MASW, CSW), and active-source microseismic surveys, utilising artificial wave generation for detailed subsurface investigations. These methods use sources such as hammer strikes, explosives, vibroseis trucks, or weight drops to generate seismic waves for detailed subsurface imaging and characterisation. Recently, seismic refraction has become increasingly popular for conducting geophysical studies on the near surface (Bery and Saad 2012). Seismic refraction methods are based on the principles of wave propagation, particularly Snell's Law to ascertain the velocity of the layer and the depths of subsurface interfaces (Brixová et al. 2018). It is widely used in geological and engineering studies to map subsurface layers, detect faults and characterise bedrock depth and quality.

SRT is especially relevant to this study due to its ability to resolve subsurface layer geometry and detect contrasts between materials such as soil, weathered rock, and bedrock. It excels in identifying velocity variations that correlate with changes in lithology, compaction, or fluid saturation, making it a valuable tool for applications like foundation assessments, landslide investigations, and aquifer studies.

Seismic refraction surveys require arrays of geophones (receivers) and seismic sources (e.g. hammer strikes or controlled explosions). The configuration of these arrays significantly influences the quality and interpretability of the data. The linear arrays involve placing geophones along a straight line, making them ideal for mapping layered structures and detecting interfaces. They provide good lateral resolution but may have limitations in capturing complex 3D geometries. These geometries can be resolved using Spread arrays which expand geophones radially or in a grid, offering better coverage. They enhance 3D imaging but require more equipment and processing time. Meanwhile, Offset arrays are used to focus on specific subsurface features by varying source and geophone positions. They are effective for capturing data near critical interfaces or fault zones.

3.2.2. SRT data acquisition

A comprehensive data acquisition process was undertaken using the Seismic Refraction Tomography (SRT) technique. Fifteen seismic lines were conducted to cover the study site. The SRT data were acquired along lines near the ERT profiles (Figure 3). The Geode seismograph (Geometrics USA), a reliable and trusted tool in the field, and 24 low-frequency geophones spaced at 5 m intervals created a spread array 115 m long. Seven shooting points were used to record the seismic data for each profile. The first shot point is 2.5 m before the first geophone, and the last is 2.5 m after the previous geophone (offset reverse shot) at 117.5 m. The rest of the shot points were 20 m apart at 17.5 m, 37.5 m, 57.5 m, 77.5 m, and 97.5 m along the line. A 10-kg sledgehammer generated compressional waves (P-waves). The number of Hummer strikes ranged between 10 and 15. The recording parameters for the SRT were a 200 msec recording length, which is the duration for which the data was recorded and a sampling interval of 0.22 μsec, which is the time between successive samples in the data. These parameters were chosen to ensure accurate and detailed data collection.

3.2.3. SRT data processing

The data are processed using the SeisImager software package to reduce noise and enhance the waveform.

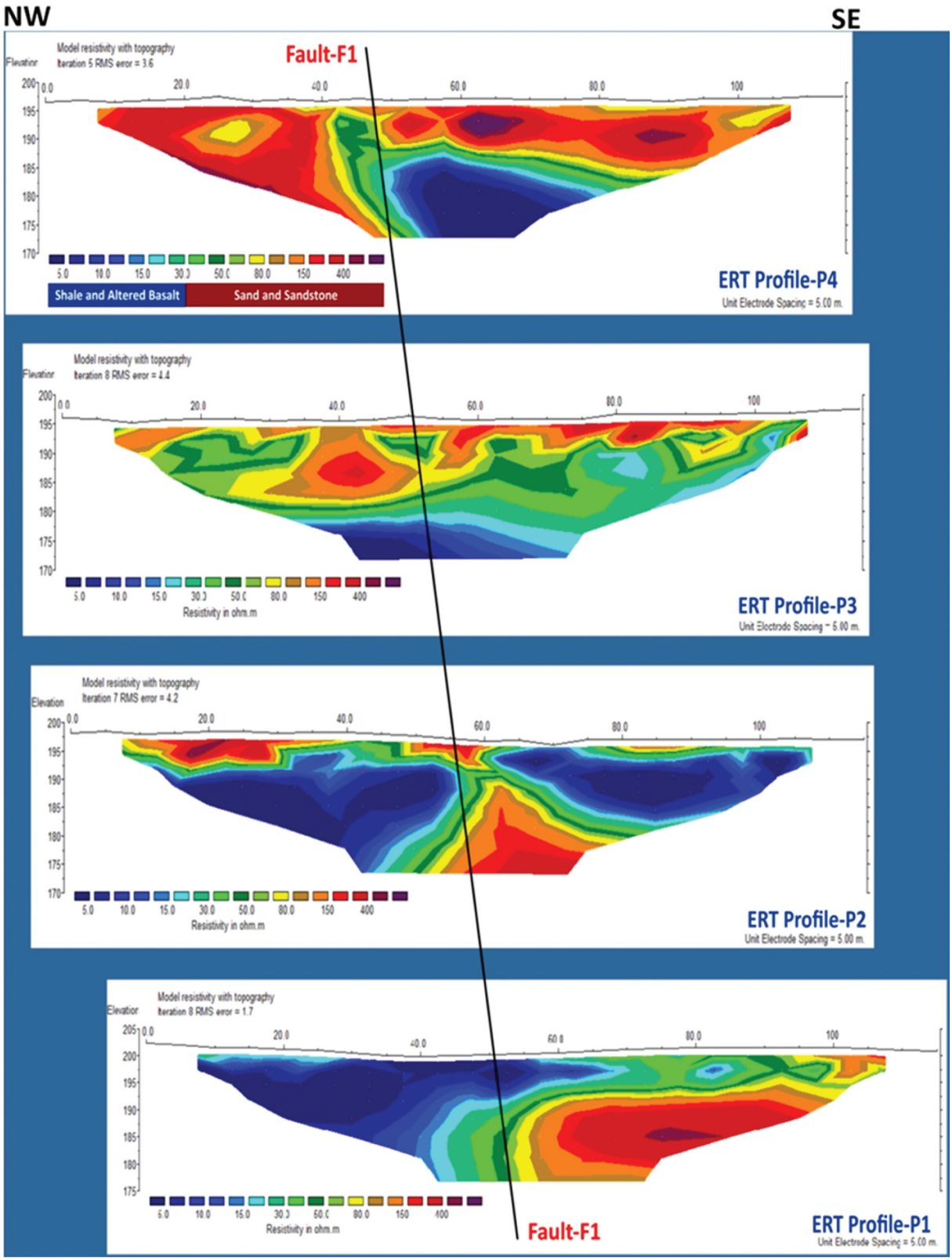

Figure 4. The inverted ERT profiles P1, P2, P3 and P4 from bottom to top respectively. These lines are crossing the fault F1.

Picking the first arrival (First breaks) is the most difficult part, and it depends on the operator's experience to identify the first breaks correctly. The picked time forms travel time curves used to perform the tomographic inversion. Tomographic inversion starts with an initial velocity model (generally generated by a simpler method like time-term inversion). Iteratively traces rays through the model to minimise the RMS error. Tomographic inversion is generally more applicable when velocity contrasts are known to be more gradational. Depending on the severity, these cases can lead to erroneous results with the common interpretation techniques (e.g. time-term and reciprocal methods).

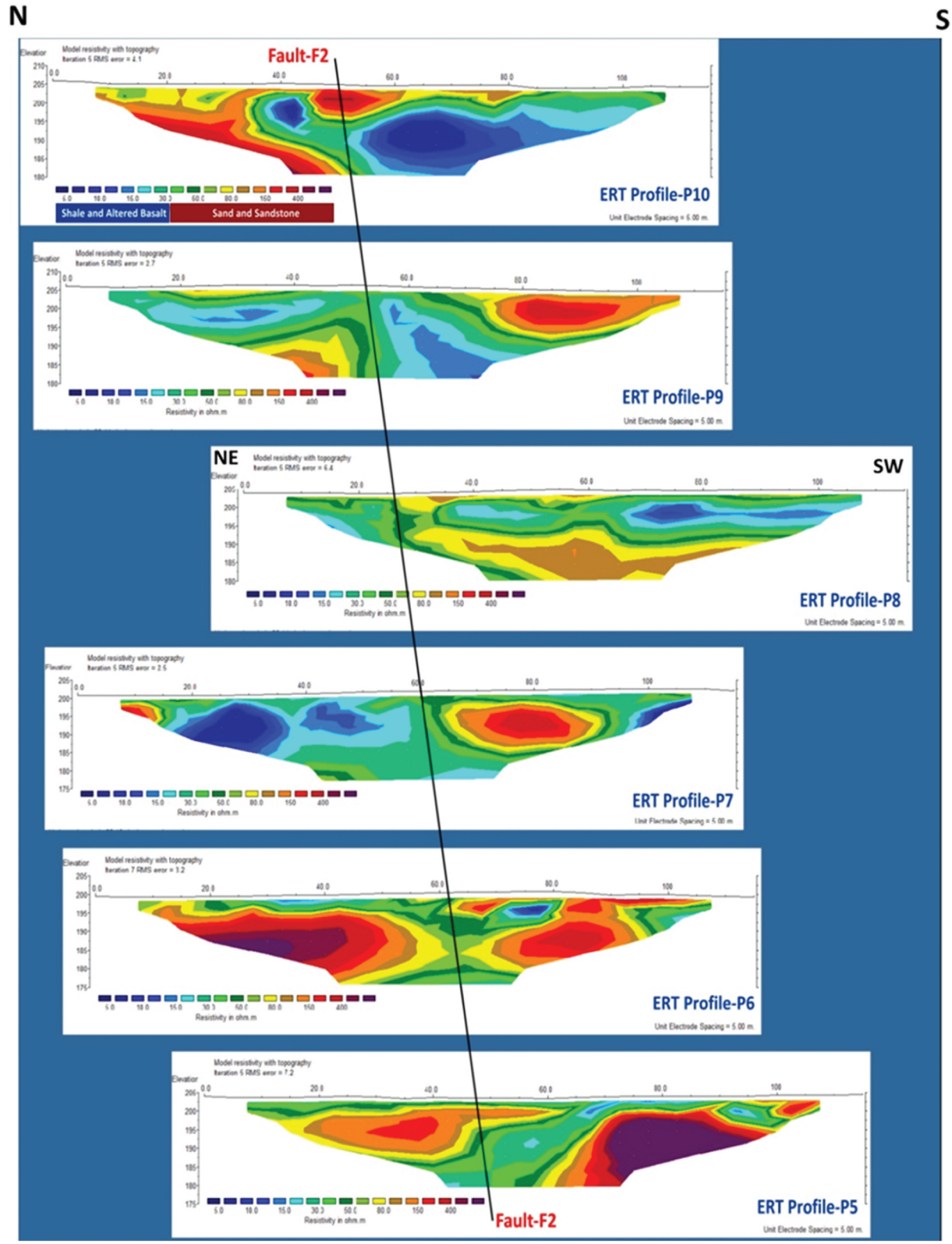

Figure 5. The inverted ERT profiles p-5 to p-10 from bottom to top respectively. These lines are crossing the fault F2.

In a tomographic inversion, the velocity model is divided into velocity "cells". All the cells have the same width, and each cell has a constant velocity. In addition, the cell height increases with depth. Then, the inversion process traces rays through the model. The inversion process evaluates the accuracy of the model by calculating the root mean square (RMS) error, which represents the total error of all the ray paths. The inversion determines the velocity of each cell at the bottom of the model but cannot estimate its height. Therefore, we intentionally removed this row of cells from the model and all the presented sections.

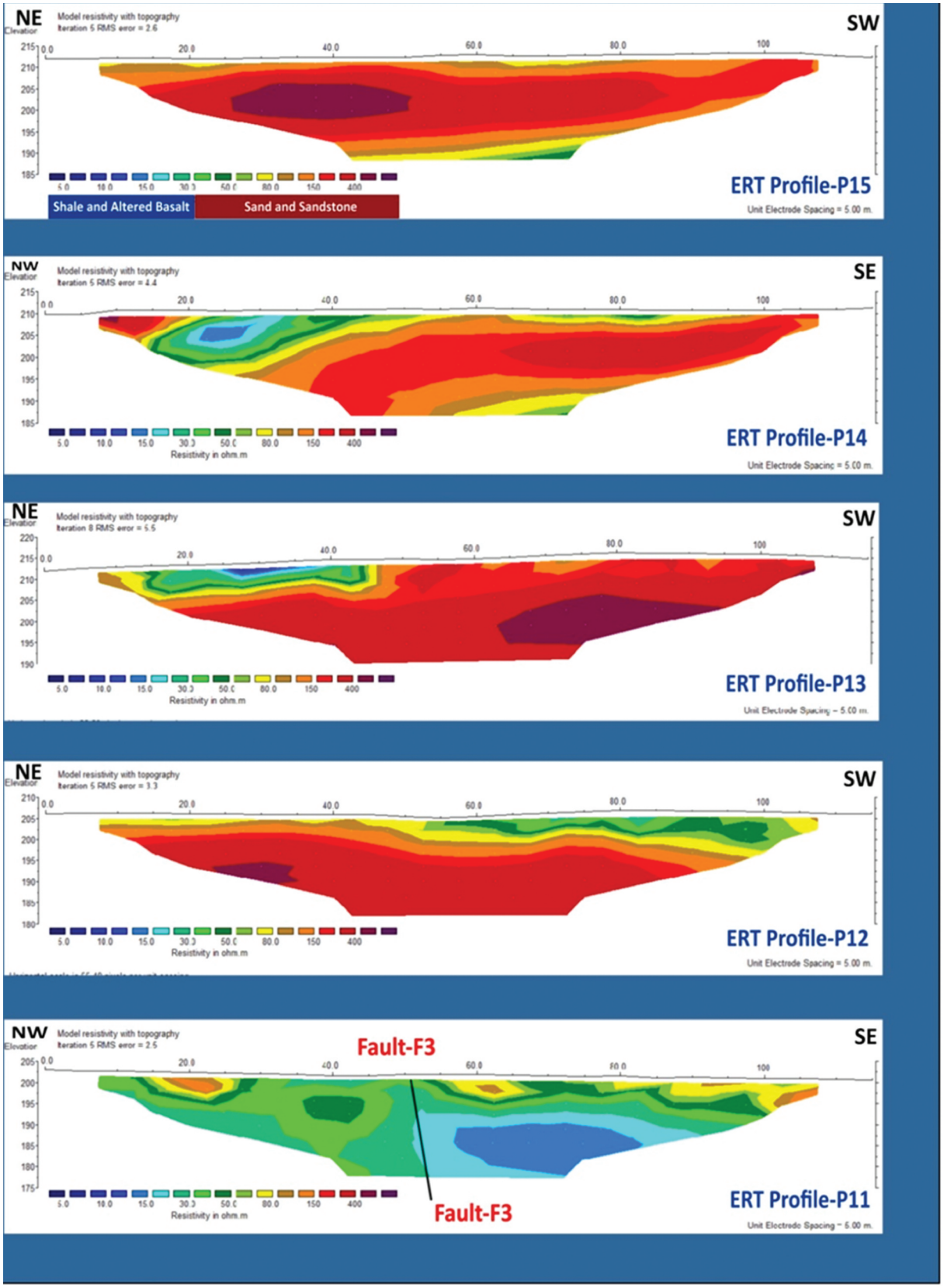

Figure 6. The inverted ERT profiles P11, P12, P13, P14 and P15 from bottom to top respectively. These lines are crossing the fault F3.

4. Results and discussion

4.1. Electrical resistivity tomography

The ERT technique has effectively identified variations in the electrical resistivity of the subsurface layers, both horizontally and vertically. These variations are related to the area's geological characteristics and can be used to differentiate between different rock types and describe the physical conditions of the subsurface layers. The ERT survey results (Figures 3–5) have identified conductive

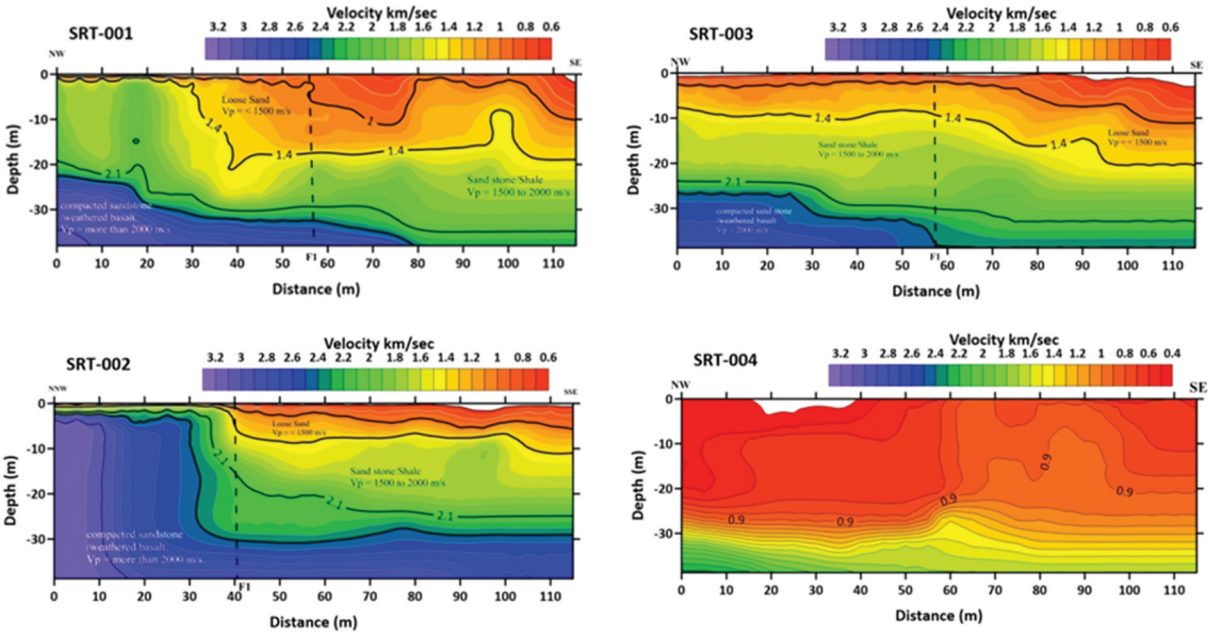

Figure 7. The estimated Vp velocity models of SRT profiles P1, P2, P3, and P4. The black dash line represents the fault-1 location as inferred from the velocity models.

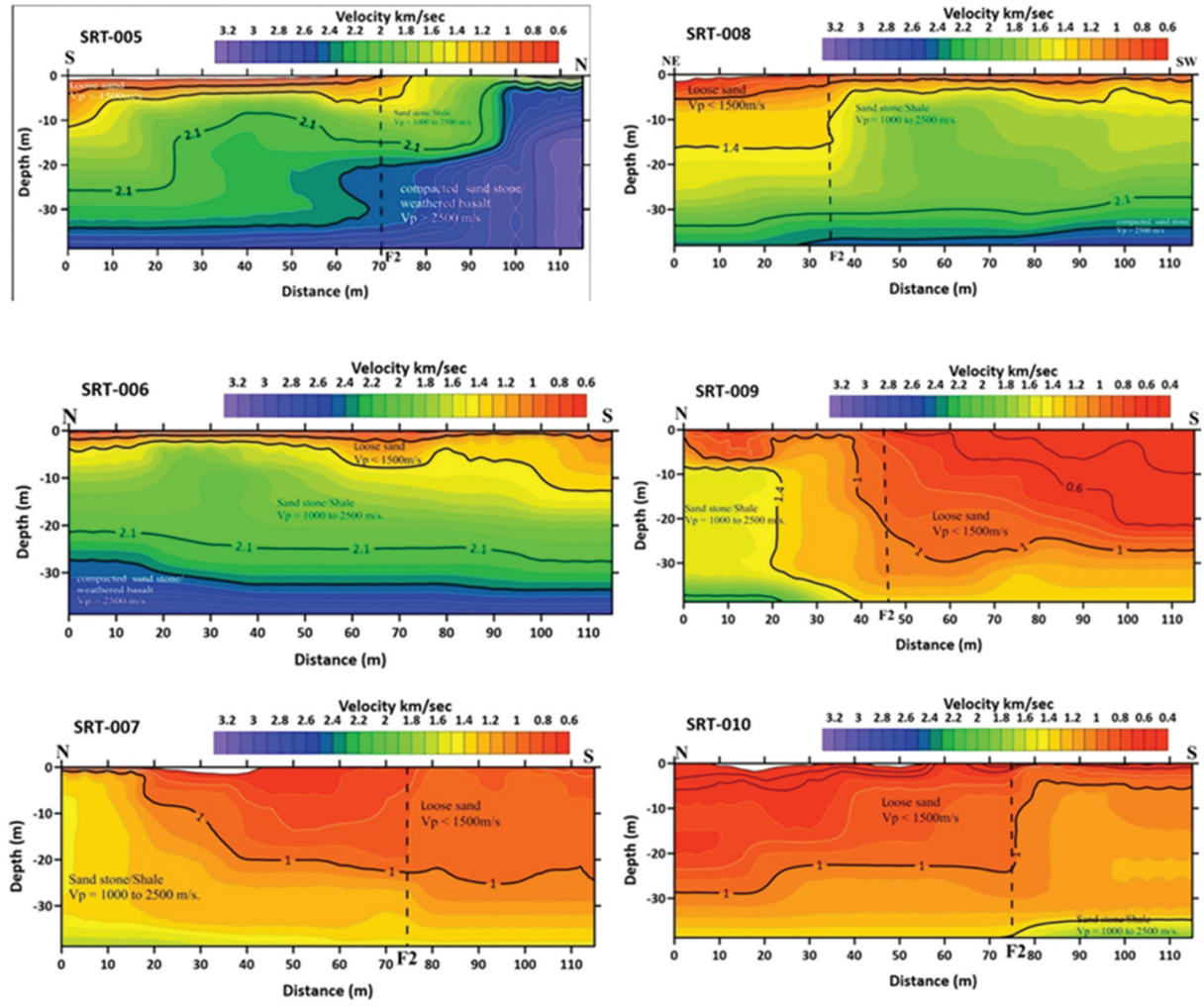

Figure 8. The estimated Vp velocity models of the SRT profiles P5 to P10. The black dash line represents the fault-2 location as inferred from the velocity models.

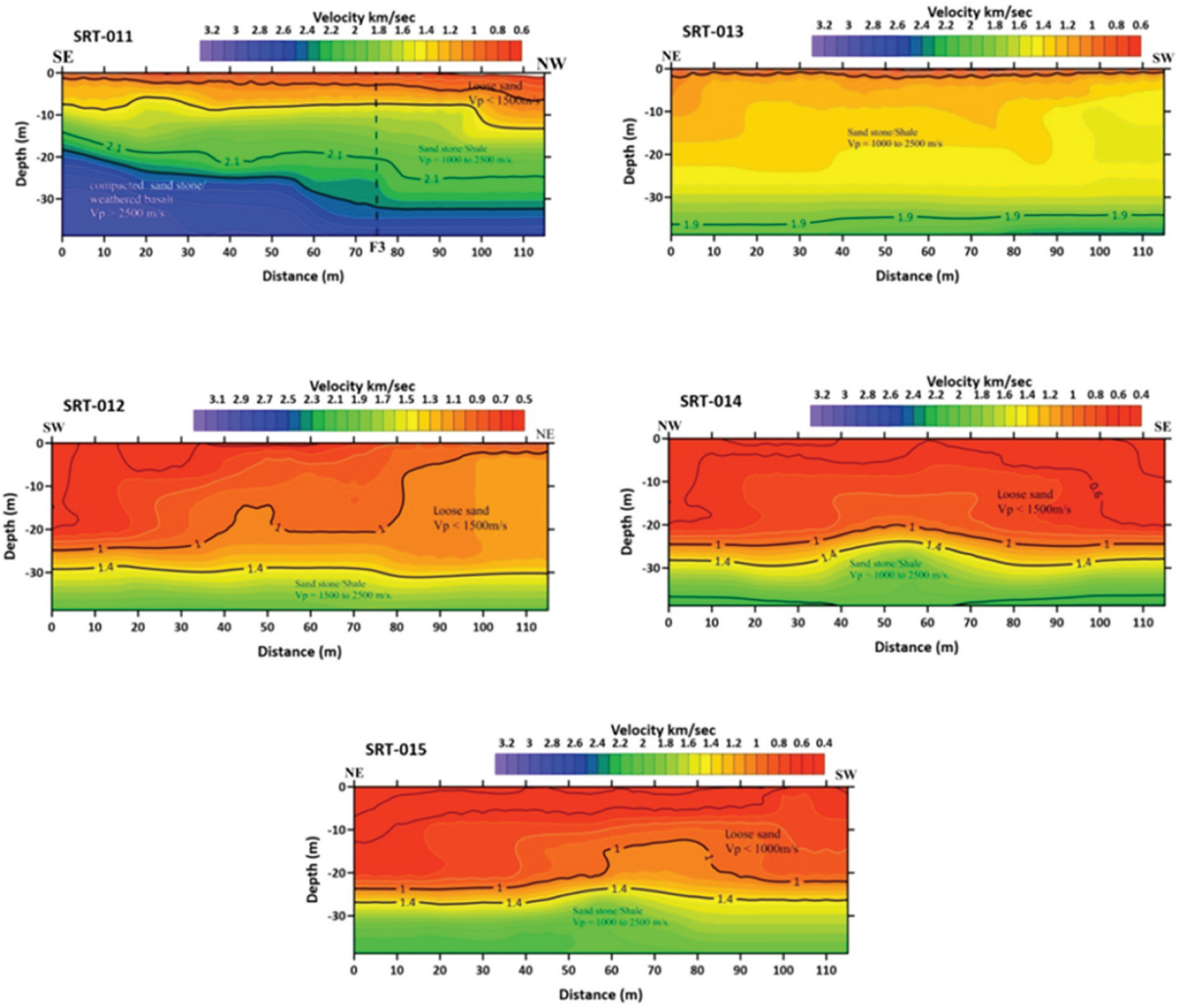

Figure 9. The estimated Vp velocity models of the SRT profiles P11 to. The black dash line represents the fault-F3 location as inferred from the velocity models.

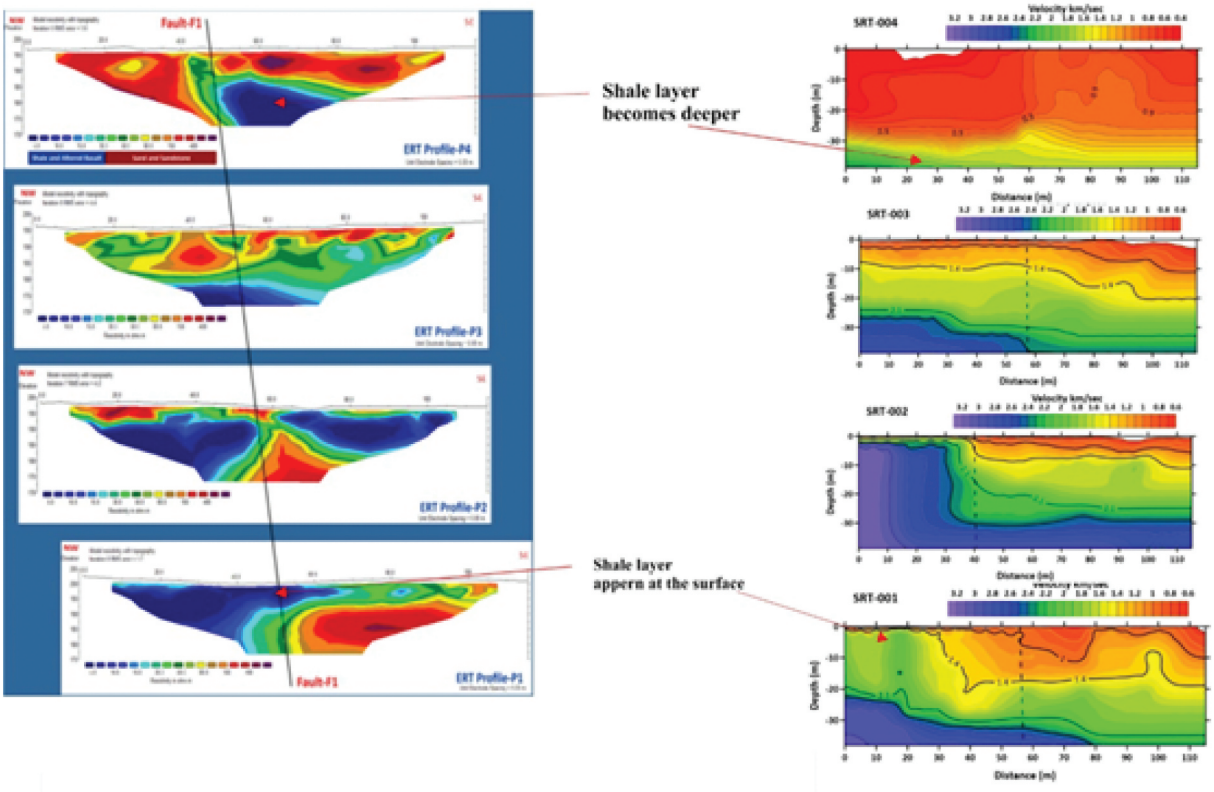

Figure 10. Shows the shale layer appear on the surface at profile P1 and become deeper at profiles P3 and P4 at the N/NE.

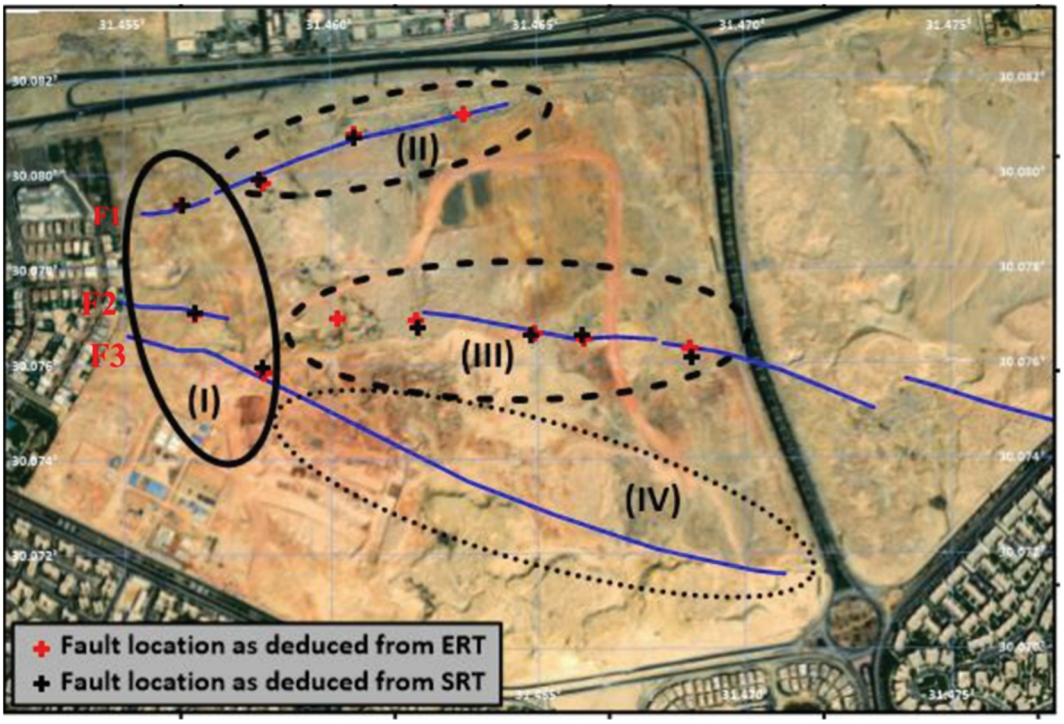

Figure 11. Locations of the obtained faults as deduced from ERT and SRT surveys. The red cross represents the fault location as deduced from the ERT while the black cross represents the fault location as deduced from the SRT.

and resistive zones. The electrically conductive zones, represented by a sky-blue colour on the 2D ERT section, can be related to the presence of shale and altered basalt. These zones have a thickness ranging from 1 to 20 m with low resistivity values of less than 50 Ω.m. The low resistivity response of shale and altered basalt could be attributed to the existence of wet soil due to near-surface water leakage and/or dominance of fine sediments. On the other hand, the resistive zones, indicated by green to dark red colours, are composed of sand and sandstone with high resistivity values exceeding 450 Ω.m. The investigated section is highly heterogeneous. So, it does not exhibit continuous layers but comprises multiple conductive and resistive zones intercalated with each other (Figures 3–5).

Furthermore, the ERT results have provided valuable insights into the arrangement of the layers. In certain sections that were examined, the sand and sandstone were found to be positioned above the shale and altered basalt. Conversely, in different sections, the shale was observed to be above the sand and sandstone profiles (P-1 and P-2). This phenomenon is attributed to the impact of three faults affecting these layers, as depicted in (Figures 4–6).

The ERT profiles successfully identified three faults that cut through the investigated sites. The first fault F1 was mapped by four ERT profiles (P1 to P4). These ERT profiles are presented in Figure 4. The western part of fault F1 was detected from the geological study and confirmed by the ERT profile P1, while the eastward extension of this fault was confirmed by the ERT profiles (P2 to P4).

The second fault F2 was mapped by six ERT profiles (P5 to P10). These ERT profiles are presented in Figure 5. The western part of fault F2 was detected from the geological study and confirmed by the ERT profile P5. The ERT survey confirmed the eastward extension of this fault through the five lines (P6 to P10).

The third fault F3 was mapped by five ERT profiles (P11 to P15). These ERT profiles are presented in Figure 6. The western part of fault F3, was detected from the geological study and crucially confirmed by the ERT profile P11 (Figure 6). In contrast, the eastward extension of this fault was not confirmed by the ERT profiles (P12 to P15).

4.2. Seismic refraction tomography

In this study, fifteen P-wave seismic refraction lines were acquired. The refraction lines provided (Vp) velocity-depth profiles that imaged the upper 30–40 m depth. Figures 7–Figure 9 show the velocity model of the seismic lines (1 to 15), respectively; see Figure 3 for SRT profiles location. The seismic velocity analysis played a pivotal role in our study, leading to the detection of three geoseismic subsurface layers.

The site has three characteristic soil lithologies:

- The upper unit (loose sand): with a variable thickness between 1 and 20 m and (Vp) values (<1500 m/s.).

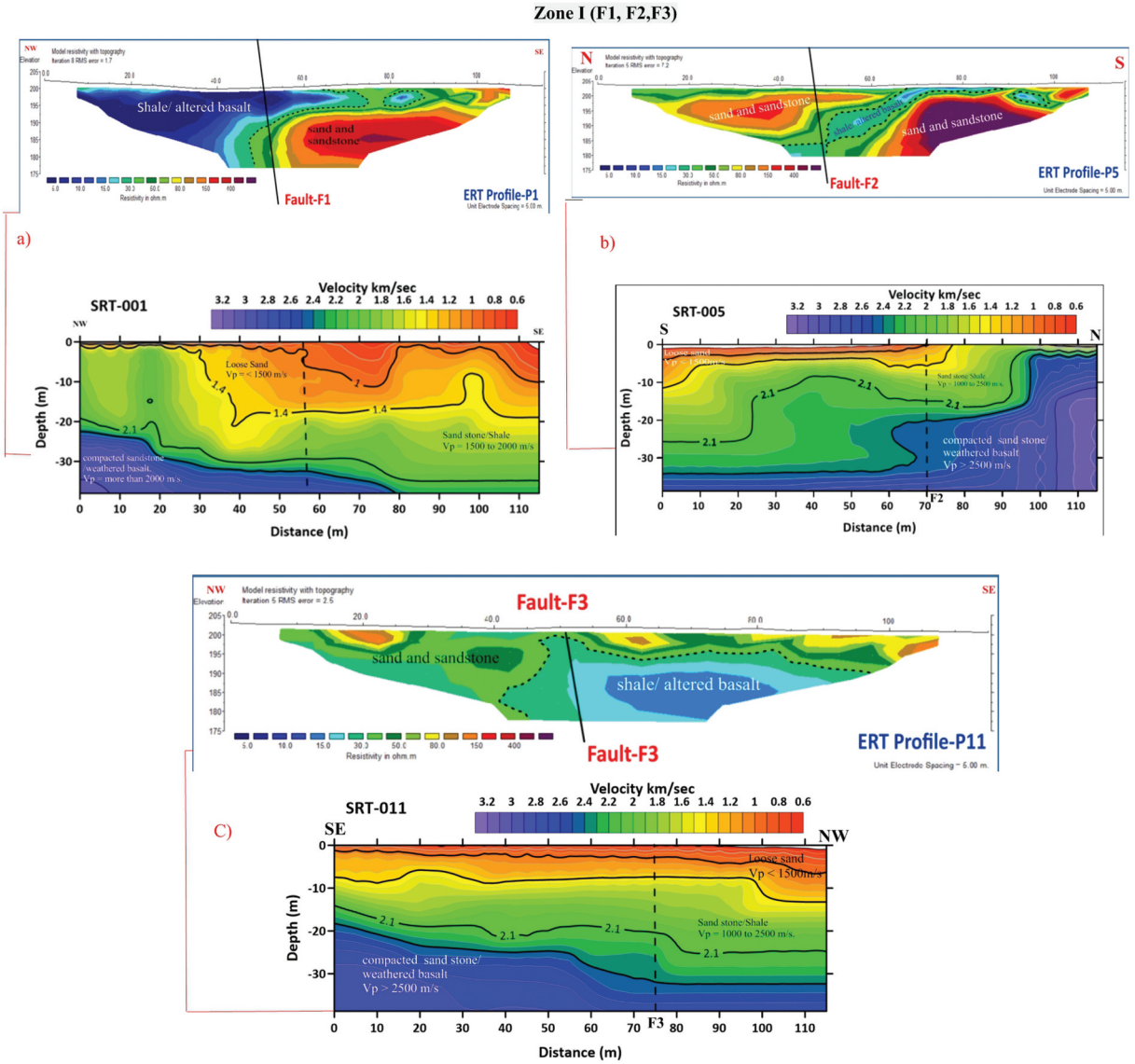

Figure 12. The ERT/SRT profiles measured in Zone I. In (A1 and B1), the ERT/SRT profile P1 confirms the presence of fault F1. In (A2 and B2), the ERT/SRT profile P5 confirms fault F2. (A3 and B3), the ERT/SRT profile P11 confirms fault F3.

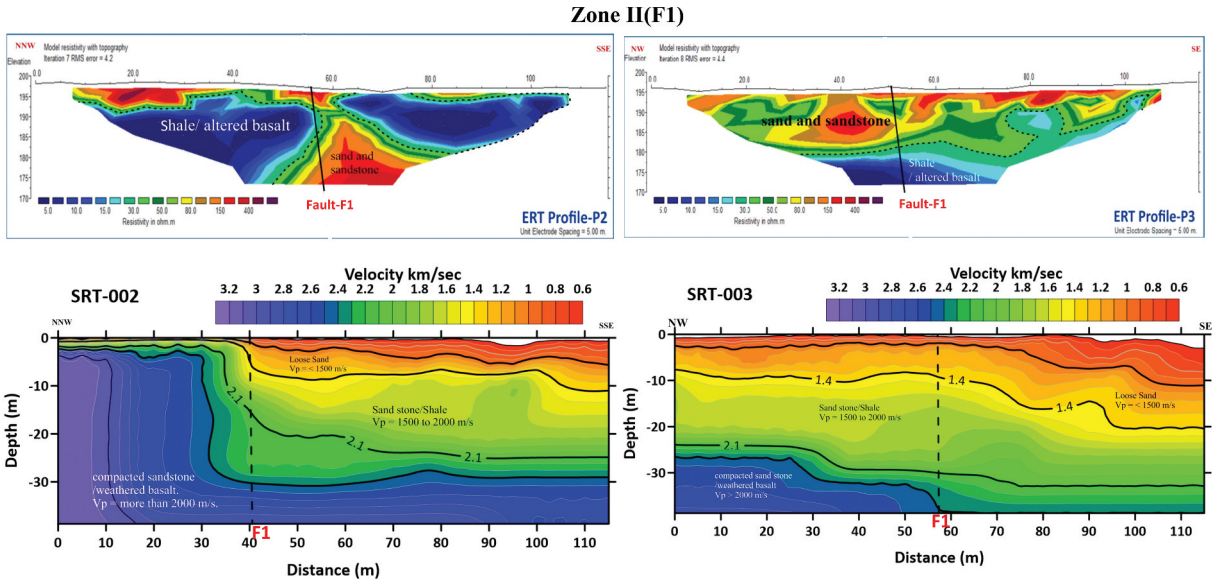

Figure 13. The ERT/SRT profiles measured in Zone II. The ERT/SRT profiles P2 and P3 confirming eastward extension of the fault F1.

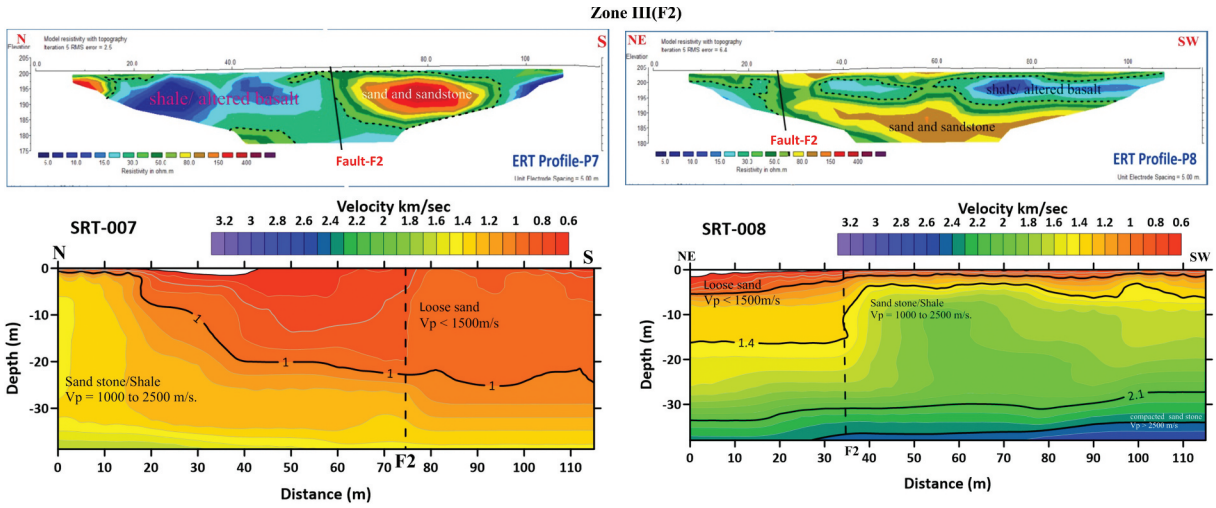

Figure 14. Some of the ERT/SRT profiles measured in Zone III. The ERT/SRT profiles P7 and P8 confirming eastward extension of the fault F2.

- The second unit (sandstone/shale): with variable thickness between 0 and 30 m). Vp velocity ranges between 1500 and 2000 m/s.
- The third unit (sandstone/weathered basalt): with a Vp velocity more than 2500 m/s.

Due to these overlapped velocity ranges, it is difficult to match the seismic refraction lines with specific lithology and to identify the layer's boundaries.

The SRT depth velocity models revealed three faults cut through the investigated site, described as follows: The fault F1 was observed through geological study. SRT confirms it through three lines (SRT-P1, SRT-P2, and SRT-P3). These lines are represented in Figure 7.

Fault F2 was inferred from the geological study, and it is confirmed by five SRT lines (SRT-P5, SRT-P7, SRT-P8, SRT-P9, and SRT-P10). These lines are represented in Figure 8.

Fault F3 was inferred from a geological study and confirmed by one SRT profile (SRT-P11) represented in Figure 9. However, the extension of the fault (F3) was not approved.

5. Integration of ERT and SRT results

The ERT and SRT results are used to estimate the geometrical parameters of the subsurface layers and outline the subsurface extension of the dominating faults. The ERT and SRT results were integrated to qualitatively determine the natural of the lithology through two different physical properties. For instance, the sand will usually have low velocity and high resistivity and in contrast the shale will have a low resistivity and high to moderate velocity.

Upon analysing the ERT and SRT results, we observed that the position of the shale layer varies from one location to the other along the study area, where it is closer to the surface in the western parts of the study area and has variable thicknesses (P-1, P5, and P-11). This layer becomes deeper towards the northeast direction (Figure 10). This condition of the shale layer is also apparent in profiles P-5 to P-10 in both ERT and SRT. This indicates that the throws of these three dominating faults are in the eastern direction.

Some shallow shale layer can pose a serious threat to buildings, highlighting the practical implications of our research. Two factors may cause impacts on the buildings, namely, the infiltration of the rainwater, irrigation water into the impermeable shale layer, where it accumulates above this layer causing rising of groundwater, which harms the buildings. Secondly, the presence of a shale layer next to the sandstone layer causes a lateral change in the foundation layers, leading to what is known as differential settlement of the construction.

The ERT and SRT techniques have played a crucial role in clarifying the fault situation at the investigated site. The results of the two data sets were consistent and showed a good match about the fault locations. Figure 11 shows the fault traces deduced from both ERT and SRT. According to the fault detection from both the geology and geophysics, the area can be divided into four zones as deduced in Figure 11.

In Zone-I the three faults were detected through the geological survey, and confirmed by the ERT and SRT results. The conducted ERT and SRT profiles in Zone I are correlated in Figure 12. These profiles appeared displacement in subsurface layers due to faults – F1, F2, and F3.

In Zones-II and Zone-III the eastward extension of the faults F1 and F2 are confirmed by the geophysical survey. The conducted ERT and SRT profiles in Zone II are correlated in Figure 13 and those of Zone III are represented in Figures 14 and 15. While, in Zone IV

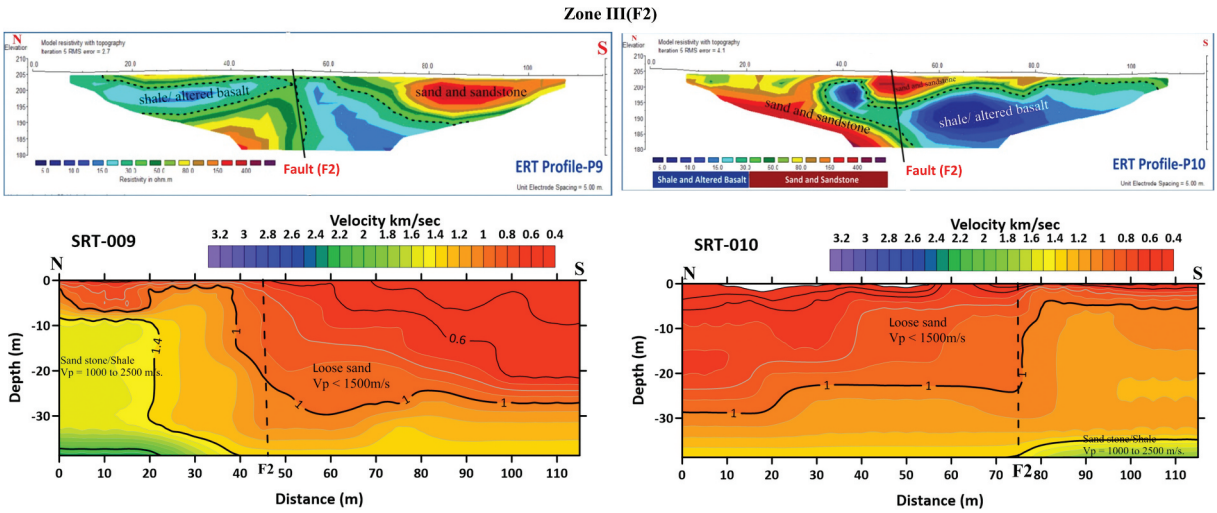

Figure 15. Some of the ERT/SRT profiles measured in Zone III. The ERT/SRT profiles P9 and P10 confirming eastward extension of the fault F2.

the geologically inferred eastward extension of the fault trace was not observed by the ERT/SRT survey.

6. Conclusion and recommendation

Electrical Resistivity Tomography (ERT) has delineated electrically conductive zones situated at different depths and composed of shale and altered basalt. These zones have a thickness ranging between 1 and 20 m and resistivity values less than 50 Ω.m. Additionally, ERT has detected a resistive zone comprising Sand and sandstone, with a thickness ranging from 1 to 20 m and resistivity values varying between 50 and 450 Ω.m at different depths. From SRT data analysis, three layers are detected based on velocity values. The first layer shows low (Vp) values (<1500 m/s) with a variable thickness of 1–20 m; it corresponds to the surface layer of loose sand. The second layer shows a relatively higher velocity between 1500 and 2500 m/s, corresponding to Sandstone/Shale with variable thickness of (1–30 m). The third layer has more than 2500 m/s, corresponding to more compacted dense Sandstone/weathered basalt.

ERT and SRT results successfully elucidated the fault configuration and its locations. Minor faults were detected at the surface during field surveying, while major structures were concealed and only outlined by the integrated ERT/SRT surveys.

The investigated site shows heterogeneous soil conditions and fault damage zones, which may impact some parts of the study area. The mapped faults bring two different rocks and soil profiles against each other, which means differential settlements of the different rock types. Hence, the building above the mapped faults is not preferred. A buffer zone of 20 m width (10 m on each side of the fault line) should be left for land scape and should not be used for construction. Moreover, lithological types must be taken into consideration, especially the weak layer. Therefore, based on the results obtained from this study, precautions must be taken into consideration before the construction of buildings. Construction design, soil replacement, and building loading should be decided by a soil engineer considering soil conditions at the fault zone.

Disclosure statement

No potential conflict of interest was reported by the author(s).

References

Abdel-Aal ME. 1982. Hydrogeological evaluation of the ground water resources in Cairo District [dissertation]. Cairo: Ain Shams University.

Ayolabi EA, Adeoti L, Oshinlaja NA, Adeosun IO, Idowu OI. 2009. Seismic refraction and resistivity studies of part of Igbogbo Township, south-west Nigeria. J Sci Res Dev. 11:42–61.

Bery AA, Saad R. 2012. Correlation of seismic P-Wave velocities with engineering parameters (N value and rock quality) for tropical environmental study. Int J Geosci. 3(4):749–757. doi: 10.4236/ijg.2012.34075.

Brixová B, Mosná A, Putiška R. 2018. Applications of shallow seismic refraction measurements in the western Carpathians Slovakia: case studies. Contrib Geophys Geod. 48(1):1–21. doi: 10.2478/congeo-2018-0001.

Elkafrawy SB, Fattah TA, Naiel T, Rashed M, Abbas AM. 2021. Environmental and site characterization investigations using remote sensing and geophysical techniques: a case from Nabq, Gulf of Aqaba, Sinai, Egypt. Remote Sens Appl. 24:100653. doi: 10.1016/j.rsase.2021.100653.

Gamal N, Yousef M, Moustafa AR, Bosworth W. 2021. Spatiotemporal evolution of transfer structures and

linked fault systems in an extensional setting. Southwest Gebel Akheider, Cairo-Suez District. Egypt Mar Pet Geol. 133:105260. doi: 10.1016/j.marpetgeo.2021.105260.

Hassan BT, Yassine M, Amin D. 2022. Comparison of urbanization, climate change, and drainage design impacts on urban flashfloods in an arid region: case study New Cairo. Egypt Water. 14(15):2430. doi: 10.3390/w14152430.

Igboekwe MU, Ohaegbuchu HE. 2011. Investigation into the weathering layer using up-hole method of seismic refraction. J Geol Min Res. 3(3):73–86.

Ismail AA, Abdelghany O. 1999. Lower Miocene foraminifera from some exposures in the Cairo-Suez District, Eastern Desert, Egypt. J Afr Earth Sci. 28(3):507–526. doi: 10.1016/S0899-5362(99)00030-5.

Lech M, Skutnik Z, Bajda M, Markowska-Lech K. 2020. Applications of electrical resistivity surveys in solving selected geotechnical and environmental problems. Appl Sci. 10(7):2263. doi: 10.3390/app10072263.

Moustafa AR. 2010. Structural setting and tectonic evolution of north Sinai folds, Egypt. Geol Soc Lond. 341(1):-37–63.. doi: 10.1144/SP341.3.

Moustafa AR, Abd-Allah A. 1991. Structural setting of the central part of the Cairo-Suez district. Mid East Res Cent. 5:133–145.

Moustafa AR, Abdel Tawab S. 1985. Morphostructures and non-tectonic structures of Gebel Mokattam. Mid East Res Cent. 5:65–78..

Okiongbo KS, Akpofure E, Odubo E. 2011. Determination of aquifer protective capacity and corrosivity of near surface materials in Yenagoa City, Nigeria. Res J Appl Sci. 3(8):785–791.

Plati C, Loizos A, Gkyrtis K. 2020. Assessment of modern roadways using non-destructive geophysical surveying techniques. Surv Geophys. 41(3):395–430. doi: 10.1007/s10712-019-09518-y.

Reynolds JM. 2011. An introduction to applied and environmental geophysics 712. (NY): John Wiley & Sons.

Said R. 1962. The geology of Egypt 377. Amesterdam (NY): Elsevier.

Sakr MA, Omar AE, Ene A, Hanfi MY. 2022. Effect of various proportions of rice husk powder on swelling soil from New Cairo City, Egypt. Appl Sci. 12(3):1616. doi: 10.3390/app12031616.

Sibul I, Plado J, Jõeleht A. 2017. Ground-penetrating radar and electrical resistivity tomography for mapping bedrock topography and fracture zones: a case study in Viru-Nigula, NE Estonia. Est J Earth Sci. 66(3):142–151. doi: 10.3176/earth.2017.11.

Steeples DW. 2001. Engineering and environmental geophysics at the millennium. Geophysics. 66(1):31–35. doi: 10.1190/1.1444910.